Volatile transport on inhomogeneous surfaces: I. Analytic expressions, with application to Pluto's day

Leslie A. Young

Southwest Research Institute, Boulder, CO, 80302

layoung@boulder.swri.edu

Submitted to Icarus 2011 Sep 8

Received_____; accepted_____;

Abstract

An analytic expression for the variation in surface and sub-surface temperature is developed for worlds whose surface pressures are nearly constant with latitude and longitude and whose atmospheres are in vapor-pressure equilibrium with the dominant surface volatiles. Such worlds include the current Pluto and Triton, and other volatile-covered Kuiper Belt Objects during some portion of their heliocentric orbit. The expressions also apply on worlds with negligible horizontal heat flow, such as asteroids. Temperature variations in volatile-covered or bare areas as a function of time is derived in terms of three thermal parameters relating to (1) the thermal wave within the substrate, (2) the energy needed to heat an isothermal volatile slab, and (3) the buffering by the latent heat needed to change the atmospheric surface pressure. For Pluto's current surface pressure (~17 μbar), atmospheric buffering dominates over subsurface effects on diurnal timescales, and should keep the surface pressure over a Pluto day constant to within 0.2%.

Keywords: Pluto, atmosphere; Pluto, surface; Atmosphere, evolution; Trans-neptunian objects

1. Introduction

Pluto, like Triton, has an N_2 atmosphere in vapor-pressure equilibrium with the N_2 ices on its surface (Owen et al., 1993). The insolation, and the temperature of the volatile ices, varies with changing subsolar latitude and heliocentric distance. Because surface pressure is an extremely sensitive function of volatile ice temperature (Brown and Ziegler 1980), the surface pressure is expected to vary by orders of magnitude over Pluto's and Triton's seasons (e.g., Trafton and Stern 1983; Hansen and Paige, 1996; hereafter HP96). In fact, factor-of-two pressure variations on decadal scales have been observed on both Pluto (Elliot et al., 2003; Sicardy et al., 2003) and Triton (Elliot et al., 1998, 2000). The observed and expected changes in Pluto's atmosphere, and the planned observations of Pluto by the New Horizons spacecraft in 2015 (Young et al., 2008), have fueled an increased interest in Pluto's changing surface and atmosphere.

For observations of the surface, detection of secular change is complicated by Pluto's variegation, with bright areas dominated by N_2-rich ices, and darker areas dominated by CH_4 or other, involatile materials (e.g., Grundy and Fink 1996). Because of the longitudinal variation, the change in observables over a Pluto day (6.4 Earth days) swamps that of the decadal variation, for Pluto's visible lightcurve (Buie et al. 2010a), infrared spectrum (Grundy and Buie 2001; Grundy et al., 2008), and thermal emission (Lellouch et al. 2011b).

Are similar diurnal variations complicating our interpretation of changes in Pluto's atmosphere? Pluto's atmosphere has been observed with stellar occultation at least once a year since 2006 (E. Young et al., 2008; Elliot et al., 2007; Buie et al., 2008; Young et al., 2009, 2010; Person et al., 2010; Olkin et al., 2011), opportunities made possible by Pluto's passage through the galactic plane (Assifin et al., 2010). The technique of stellar occultations is currently the most sensitive method for measuring the changes in Pluto's atmosphere. The

high cadence of Pluto stellar occultations allows additional comparisons at the timescales of months. It has been argued elsewhere (Stern and Trafton 1984; Spencer et al., 1997) that Pluto's surface pressure and volatile ice temperature should be nearly uniform *spatially* if the atmosphere is dense enough to effectively transport mass from areas of sublimation to areas of deposition. I ask a different, but related, question. If Pluto's atmosphere has a single surface pressure at any given time, how does that surface pressure change as Pluto rotates, so that different portions of Pluto's voltiless are illuminated? In other words, is there a dependence on the subsolar longitude?

In investigating the question of Pluto's diurnal variation, I derive an analytic expression involving dimensionless thermal parameters analogous to those used by Spencer et al. (1989) for a homogeneous, volatile-free surface. The work of Spencer et al. (1989) has been widely cited, showing the utility of such thermal parameters as an aid to intuitive understanding. By including these thermal parameters in an analytical expression, their utility is extended even further, for quick investigations of the effects of different physical assumptions, and as initial conditions for numerical models.

In Section 2, I derive these thermal parameters and analytical expressions for volatile ice temperatures. I apply these parameters to the case of Pluto's diurnal variation in Section 3, and compare the expressions to previous work in Section 4.

2. Analytical expressions for surface temperatures

The conceptual framework for the model presented here is built on the physical processes considered by Hansen and Paige 1992 and Hansen and Paige 1996 (HP96), as illustrated in Fig 1. These include thermal conduction into and within a substrate, an internal heat flux, absorbed sunlight, and thermal emission. For the analytic solution, the thermophysical parameters of the substrate (specific heat, c; thermal conductivity, k; and density, ρ) are assumed to be constant with depth and with time, but are allowed to vary from location to

location. The lower boundary condition balances conduction with an internal heat flux, *F*. Because the diurnal thermal wave only penetrates to a small fraction of the depth of the seasonal thermal waves (HP96), the internal heat-flux term can be used to model diurnal variation superimposed on a seasonal cycle. The emissivity, ε, is also taken to be variable in location but constant in time.

INSERT FIG 1 HERE

This model, like that of HP96, assumes that the volatile ice temperature is the same everywhere on the planet. This assumption is discussed in detail elsewhere, such as Spencer et al., (1997). In brief, if the atmosphere is dense enough to effectively transport mass from sublimation zones to condensation zones, it also transports energy in the form of latent heat. This mechanism becomes ineffective when the winds transport the needed mass approach the sound speed (Trafton and Stern, 1983). Spencer et al., (1997) estimate that Pluto is in the global-atmosphere regime for pressures greater than 60 nbar (N_2 ice temperatures greater than 30.5 K). Since Pluto's atmosphere has been measured directly by stellar occultations to be higher than 7 μbar (E. Young et al., 2008), Pluto is firmly in the global-atmosphere regime.

As in HP96, this model assumes that the volatile ice* forms slabs that are isothermal with depth, as well as with latitude and longitude, essentially equivalent to assuming that the N_2 grains within the slab are in vapor pressure equilibrium with the atmosphere (Grundy and Stansberry, 2000). Within the volatile ice slab, a net energy source will lead to an increase in the volatile temperature. The N_2 ice in the diurnal scenario considered here does not cross the α-β phase transition of N_2 at 35.61 K (Brown and Zeigler 1980), and the latent heat of the solid phase transition is this not included in this model.

* In previous work (e.g., HP96), the condensed volatile is referred to as *frost*. The term *volatile ice* or simply *volatile* is used here instead, since the term *frost* should be reserved for the condensation of a minor gaseous species diffusing through a major species (Grundy 2011).

Although the latitudinally averaged volatile-transport problem has been previously implemented numerically (e.g., Moore and Spencer 1990, HP96), there is still value in an analytic expression for the volatile transport on a latitudinally inhomogeneous surface. First, simple analytic expressions provide physical insight into the dominant physical processes in a problem. Second, analytic expressions provide useful diagnostics when constructing new numerical models. Third, analytic expressions can provide sensible initial conditions for numerical calculations.

To make this problem amenable to an analytic solution, elements on the surface are described as either volatile-covered or volatile-free. This is a simplification for two reasons. The first is that the surface of Pluto consists of the volatile species CO and CH_4 as well as N_2. A volatile-transport model that includes these minor species will be an important extension, especially for understanding the evolution of the atmospheric composition of volatile-covered bodies such as Pluto and Triton. However, while multi-component volatile ices can radically alter the surface pressure in some cases, through the formation of a CH_4 or CO rich crust (Trafton 1990), it appears as though any such crust on Pluto or Triton, if present, is not rich enough in the minor species to shut off the communication of N_2 with the atmosphere (Lellouch et al. 2009, 2011a). Therefore, the usual assumption (HP96, Spencer et al., 1997), that the atmospheric N_2 is in vapor-pressure equilibrium with the N_2 ice, appears valid. Therefore, for application to Pluto or Triton, "volatile-covered" refers to areas of N_2-dominated ices, while "volatile-free" refers to both CH_4-dominated area, and areas devoid of volatiles. The second reason why describing an area on the surface as either volatile-covered or volatile-free (that is, a static composition model) is a simplification is that, in reality, volatiles are free to move around the surface. For Pluto's diurnal cycle, the net sublimation or deposition (~10 micron) is a small fraction of the N_2 grain size (Grundy and Stansberry 2000), justifying this static description of the volatile distribution. A static distribution is less valid at decadal timescales, as N_2 is transported from areas of net sublimation to net

deposition. For example, in run #12 of HP96, areas of the sunlit pole become volatile-free at a rate of 1% of Pluto's total surface area per year in the current post-perihelion epoch. Over seasonal timescales, a static distribution is only valid if a surface is an "ice ball" that is entirely covered in volatiles, or if high substrate thermal inertia leads to a static volatile distribution (e.g., the "Koyaanismuuyaw" model of hemispherical dichotomy of Moore and Spencer 1990, or run # 32 of HP96).

Given solar forcing that repeats over a period P, we are looking for periodic solutions of the surface temperatures. The simplest such solution is one where the absorbed insolation, S, and volatile temperature, T_V, are expressed as the sum of a constant term and a sinusoidal term. This is most compactly expressed in its complex form:

$$\begin{aligned} S(t,\lambda,\phi) &= S_0 + S_1(\lambda,\phi)e^{i\omega t} \\ T_V(t) &= T_{V0} + T_{V1}e^{i\omega t} \end{aligned} \tag{1}$$

where t is time, $\omega = 2\pi/P$ is the frequency, λ is latitude, and ϕ is longitude. As usual for the complex representation of wave equations, the real part is taken for the physical quantities. Higher frequencies can easily be included to more accurately reflect the true variation of the solar forcing.

The temperature within the substrate, T_S, satisfies the diffusion equation, $\rho c \dot{T}_S = k\partial^2 T_S/\partial z^2$ (HP96), where dotted variables indicate derivative with respect to time, and z is the height above the substrate surface (zero at the top of the substrate, decreasing downward). At the boundary between the substrate and the volatile slab, the substrate temperature equals the slab temperature. At the lower boundary, $k\partial T_S/\partial z = -F$. A temperature profile that satisfies the diffusion equation and the boundary conditions has the solution

$$T_S(z,t) = -(F/k)z + T_{S0} + T_{S1}e^{i\omega t + (\sqrt{i\omega}\Gamma/k)z} \tag{2}$$

where $\Gamma = \sqrt{k\rho c}$ is the thermal inertia, introduced to simplify later expressions. The skin depth, l_s, as defined by Spencer et al. (1989) and HP96, is $l_s = k/(\Gamma\omega^{1/2})$. Since $\sqrt{i} = (1+i)/\sqrt{2}$, the time-variable term describes a damped oscillation, with wavelength $2\pi\sqrt{2}l_s$ and e-folding distance of $\sqrt{2}l_s$.

As illustrated in Fig. 1, heating of the volatile slab depends on solar insolation (always a source), thermal emission (always a sink), thermal conduction to the substrate (a sink if the volatile slab is warmer than the substrate), and latent heat (positive for deposition, or $\dot{m}_V > 0$).

$$c_V m_V \dot{T}_V = S - \varepsilon\sigma T_V^4 - k\left.\frac{\partial T_S}{\partial z}\right|_{z=0} + L\dot{m}_V \tag{3}$$

where c_V is the specific heat of the volatile slab, m_V is the column mass of the volatile slab, ε is the thermal emissivity, σ is Stefan-Boltzmann constant, L is the latent heat of sublimation, and S is the absorbed insolation, given by $S = \left(S_{1AU}/\Delta^2\right)\cos\theta(1-A)$. S_{1AU} is the normal insolation at 1 astronomical unit (AU), Δ is the heliocentric distance in AU, θ is the incidence angle, and A is the wavelength-averaged hemispheric albedo (Hapke 1993). This expression ignores the effects of surface roughness on the surface temperature (Spencer 1990). The temperature derivative is calculated at top of the substrate, at $z = 0$.

The spatial average over the volatile-covered areas is denoted by angled brackets. For example, the insolation averaged over the volatiles is

$$\langle S(t)\rangle \equiv \frac{1}{4\pi f}\int_{volatile} S(t,\lambda,\phi)\cos\lambda\, d\lambda\, d\phi \tag{4}$$

where f is the fractional area covered by volatiles, λ is latitude, and ϕ is longitude. Global energy balance is then found by averaging the local energy balance (Eq. 2) over the volatiles:

$$\langle c_V m_V\rangle \dot{T}_V = \langle S\rangle - \langle\varepsilon\rangle\sigma T_V^4 - \left\langle k\left.\frac{\partial T_S}{\partial z}\right|_{z=0}\right\rangle + L\left\langle \dot{m}_V\right\rangle \tag{5}$$

where we have used the fact that T_V is constant over all the areas covered by volatiles.

To proceed further, we need to eliminate the final term, $L\left\langle \dot{m}_V \right\rangle$. This is sometimes achieved by imposing $\dot{m}_V = 0$, or global balance of sublimation and deposition (e.g., Moore and Spencer 1990). It is more correct to consider global mass balance, including the change in the atmospheric bulk (e.g., HP96). The equation for global mass balance is

$$f\left\langle \dot{m}_V \right\rangle + \dot{m}_A + \dot{m}_E - \dot{m}_S = 0 \tag{6}$$

where m_A is the column mass of the atmosphere (assumed to be globally uniform), $\dot{m}_E$ represents the escape rate, in units of mass per area per time, and $\dot{m}_S$ represents sources other than that from the volatile ice slab, such as geysers, averaged over the entire surface. As with the volatile temperature and solar forcing, the escape rate and other sources are expressed as a sinusoid, as $\dot{m}_V = \dot{m}_{V0} + \dot{m}_{V1} e^{i\omega t}$ and $\dot{m}_S = \dot{m}_{S0} + \dot{m}_{S1} e^{i\omega t}$, where $\dot{m}_{V1}$ and $\dot{m}_{S1}$ are complex numbers.

Assuming hydrostatic equilibrium, vapor-pressure equilibrium, and the Classius-Clapeyron relation, the column mass of the atmosphere is a function of the surface temperature, so the change in the atmospheric column mass can be expressed as

$$\left\langle \dot{m}_A \right\rangle = \frac{dm_A}{dT_V} \dot{T}_V \tag{7}$$

where

$$\frac{dm_A}{dT_V} = \frac{1}{g} \frac{dp_{surf}}{dT_V} = \frac{1}{g} \frac{L_T p_0}{T_V^2} \exp\left[L_T \left(\frac{1}{T_{V0}} - \frac{1}{T_V} \right) \right] \tag{8}$$

p_{surf} is the surface pressure. g is the effective gravitational acceleration, defined by $g = p_{surf} / m_A$. For bodies with large scale heights, H, such as Pluto, this includes an adjustment to the gravitational acceleration at the surface, $g_{\rm surf}$, so that $g = g_{\rm surf}$ (1 - 2 H/R). L_T is latent heat expressed in units of temperature ($L_T = L\mu m_{amu} / k_{\rm B}$, where μ is the molecular weight, m_{amu} is the atomic mass unit, and $k_{\rm B}$ is Boltzmann constant. For N_2 at 37.9 K, L_T = 852.7 K). L_T is introduced purely for notational convenience. p_0 is the equilibrium vapor pressure at T_{V0}.

Substituting Eqs. 6 and 7 into Eq. 5 gives a new form of the global energy equation:

$$\left(\langle c_V m_V \rangle + \frac{L}{f}\frac{dm_A}{dT_V}\right)\dot{T}_V = \langle S \rangle - \langle \varepsilon \rangle \sigma T_V^4 - \left\langle k \left.\frac{\partial T}{\partial z}\right|_{z=0} \right\rangle + \frac{L}{f}\left(\dot{m}_S - \dot{m}_E\right) \tag{9}$$

We substitute the sinusoidal expressions for T_V and S (Eq. 1) into Eq. (9) and expand to first order. The time-averaged form of Eq. (9) becomes

$$0 = \langle S_0 \rangle - \langle \varepsilon \rangle \sigma T_{V0}^4 + \langle F \rangle + \frac{L}{f}\left(\dot{m}_{S0} - \dot{m}_{E0}\right) \tag{10}$$

which simply states that the thermal emission balances solar insolation, internal heat flux, and the latent heat associated with atmospheric sources and sinks. By restricting the expansion to first order, we are ignoring cross terms T_V^4 that depress the mean temperature in the case of small thermal inertia, as seen in Spencer et al., (1989). This is discussed further in Section 3.

The time-varying portion of Eq. (9), or those terms proportional to $e^{i\omega t}$, are

$$\left(\langle m_{V0} c_V \rangle + \frac{L}{f}\frac{dm_A}{dT_V}\right) i\omega T_{V1} = \langle S_1 \rangle - 4\langle \varepsilon \rangle \sigma T_{V0}^3 T_{V1} - \sqrt{i\omega}\langle \Gamma \rangle T_{V1} + \frac{L}{f}\left(\dot{m}_{S1} - \dot{m}_{E1}\right) \tag{11}$$

Eq. (11) is written more simply by defining three thermal parameters (Eqn. 12-14). The first, Θ_S, describes the modulation to the volatile ice temperature from thermal conduction into and out of the substrate (subscripted *S* for substrate). This parameter is analogous to the thermal parameter defined in Spencer et al. 1989, where we use the mean volatile temperature, T_{V0}, rather than the sub-solar equilibrium temperature used by Spencer et al. 1989.

$$\Theta_S(T) = \frac{\sqrt{\omega}\langle \Gamma \rangle}{\langle \varepsilon \rangle \sigma T^3} \tag{12}$$

The second thermal parameter, Θ_V, describes the modulation to the volatile temperature due to the thermal inertia of the isothermal volatile ice slab (subscripted *V* for volatile slab).

$$\Theta_V(T) = \frac{\omega \langle m_{V0} c_V \rangle}{\langle \varepsilon \rangle \sigma T^3} \tag{13}$$

The final parameter, Θ_A, describes how the atmosphere buffers the volatile ice temperature due to the latent heat needed to change the atmospheric pressure in response to the volatile ice temperature (subscripted *A* for atmosphere).

$$\Theta_A(T) = \omega \frac{L}{f} \frac{dm_A(T)}{dT_V} \frac{1}{\langle \varepsilon \rangle \sigma T^3} \tag{14}$$

With these three parameters, the variation in the temperature can be written to first order as

$$T_{V1} = \frac{\langle S_1 \rangle + \frac{L}{f}\left(\dot{m}_{S1} - \dot{m}_{E1} \right)}{4 \langle \varepsilon \rangle \sigma T_{V0}^3} \frac{4}{4 + \sqrt{i}\Theta_S(T_{V0}) + i\left(\Theta_V(T_{V0}) + \Theta_A(T_{V0})\right)} \tag{15}$$

As usual, the real part of the complex expression is taken as the physical quantity. The first term represents the variation in the equilibrium temperature, $T_{V1,\mathrm{eq}}$, or the time-dependant portion of the volatile temperature in instantaneous balance with the insolation, internal flux, and escape and other mass source terms.

A similar derivation applies to volatile-free regions, where the mass of the volatile slab is zero and there is no latent heat term in the local energy balance equation (Eq. 3). In this case, there is no communication between the volatile-free surface elements. Writing the local volatile-free surface temperature as $T(t) = T_0 + T_1 e^{i\omega t}$, the volatile-free equation for the time-averaged temperature (equivalent to Eq. 8) is

$$0 = S_0 - \varepsilon \sigma T_0^4 + F, \text{ volatile free} \tag{16}$$

and the volatile-free variation is, analogous to Eq. (14),

$$T_1 = \frac{S_1}{4\varepsilon\sigma T_0^3} \frac{4}{4 + \sqrt{i}\Theta_S(T_0)}, \text{ volatile free} \tag{17}$$

where the thermal parameter Θ_S is calculated using local values of Γ, ε, and T_0.

The three thermal parameters derived here allow a quick intuitive insight into the effect of thermal inertia and atmospheric buffering. As described by Spencer et al. (1989), small values of the thermal parameters leads to temperatures that strongly track the solar input with only small phase lags, while large thermal parameters strongly suppress the temperature variation and leads to a phase lag that tends to an asymptotic value (Table I). The amplitude of the temperature variation is suppressed by a factor *a*:

$$a = \frac{T_{V1}}{T_{V1,eq}} = \frac{4}{\sqrt{\left(4 + \Theta_S/\sqrt{2}\right)^2 + \left(\Theta_V + \Theta_A + \Theta_S/\sqrt{2}\right)^2}} \tag{18}$$

The phase lag, ψ, expressed in radians, can be derived from the real and imaginary parts of the denominator in Eq. (15), so that

$$\psi = \arctan\left(\frac{\Theta_V + \Theta_A + \Theta_S/\sqrt{2}}{4 + \Theta_S/\sqrt{2}}\right) \tag{19}$$

The relaxation timescale is the characteristic timescale for the temperature to relax to a new equilibrium. The derivation for the timescale proceeds analogously as above, expressing the temperature as $T_V(t) = T_{V0} + T_{V1}e^{-t/\tau}$. The timescale is then easily expressed in terms of Θ_V, Θ_V and Θ_A.

$$\tau = \frac{1}{\omega}\left(\frac{\Theta_V}{4} + \frac{\Theta_A}{4} + \frac{\Theta_S}{4\sqrt{2}}\right) \tag{20}$$

INSERT TABLE I HERE

Eqs. (10) and (15) are used to find the variation of volatile temperature with time. I emphasize that this formulation describes the variation of the volatile temperature with *time*, while maintaining usual assumption that the volatile temperature is *spatially* isothermal.

Returning to the local energy equation, Eq. (3), we can derive the equation for the local sublimation rate of latent heat averaged over a period. This is simply the local energy input minus the energy input averaged over the volatiles.

$$-L\dot{m}_{V0} = (S_0 + F) - \left(\langle S_0 \rangle + \langle F \rangle + \frac{\dot{m}_{S0} - \dot{m}_{E0}}{f} \right) \quad (21)$$

The time-varying portion of the sublimation rate is similarly related to the time-varying difference between the local insolation and that averaged over the volatile areas.

$$-L\dot{m}_{V1} = S_1 - \langle S_1 \rangle + \frac{i\Theta_A}{4 + \sqrt{i}\Theta_S + i\Theta_V + i\Theta_A} \langle S_1 \rangle \quad (22)$$

If the time-varying average insolation ($<S_1>$) is small, or if Θ_A is large, then the local sublimation rate balances the variation of the local insolation. If Θ_S or Θ_V are large and Θ_A is small, so that temperatures are buffered by something other than the atmosphere, then the local sublimation rate balances the difference between local and global insolation.

3. Application to Pluto

This work was motivated by the question of whether or not we expect to see variation in Pluto's N_2 ice temperature, and surface pressure, over the course of a Pluto day. To address this question, I consider the constraints on Pluto's thermal inertia derived from its thermal emission by Lellouch et al. (2011b; hereafter L11). L11 considered several composition maps, including the map of Grundy and Fink (1996). For this map, L11 use A = 0.67, ε = 0.5, and T_V = 37.4. These are not self-consistent; that is, the insolation averaged over the N_2 ice, (1-A)$<S_0>$, is 107 erg cm^{-2} s^{-1}, while the thermal emission, $\varepsilon\sigma T_V^4$, is only 78 erg cm^{-2} s^{-1}. For this analysis, I chose similar, but self-consistent, parameters: A = 0.8, ε = 0.55, and T_F = 37.87 K. The result, that Pluto's atmosphere is constant over a day to better than 1%, is robust to details of the choices of albedo, emissivity, and heat flux, as described below.

INSERT FIG 2 HERE

In the Grundy and Fink (1996) composition map, the N_2-rich terrain covers 53% of the total area of Pluto, but is unevenly distributed (Fig 2A). As seen from the Sun in 2011, the

N_2-rich areas cover 65% of the visible disk at a longitude of 151° (IAU)*, near lightcurve maximum (Buie et al. 2010a), but only 41% at a longitude of 283° (IAU), near lightcurve minimum (Fig 2B). If the N_2 ice temperature were such that the thermal emission was in instantaneous equilibrium with the insolation averaged over the volatiles (e.g., $\varepsilon\sigma T_{V,eq}^4 = (1-A)\langle S(t)\rangle$), then the N_2 ice temperatures would range from 36.0 to 40.2 K. The pressure is a sensitive function of temperature, and this 4.2 K peak-to-peak variation (Fig 2C) implies that the surface pressure would vary by a factor of 12 (Table II). This huge range of variation is not seen in the history of Pluto occultations (e.g., Young et al. 2010, Person et al. 2010).

INSERT TABLE 2 HERE

I next consider the thermal inertia of the substrate, adopting a thermal inertia of $1.8\text{x}10^4$ erg cm^{-2} s^{-1} $\text{K}^{-1/2}$ based on Lellouch et al. 2011. This gives a diurnal thermal parameter for the substrate, Θ_S, of 36. This is larger than the values of $\Theta(\square_{\square\square})$~5-12 in L11 for the CH_4-rich and tholin areas because that is calculated for the equilibrium sub-solar temperature of 63.3 K, rather than for T_{V0} = 37.9 K. The thermal inertia decreases the temperature variation of the N_2 ice by roughly a factor of 9 (or $\Theta_s/4$), for a 0.4 K peak-to-peak range (Fig 2D). While much smaller than the variation for equilibrium temperatures, this is still large enough for the surface pressure to vary by 27%. This is precisely the order of variation that motivated this work. However, the two other effects, the thermal inertia of the volatile slab and the atmospheric buffering, decrease this variation still further.

An isothermal N_2-ice slab, with $c_V = 1.3\text{x}10^7$ erg g^{-1} (Spencer et al., 1992), and m_V = 9.5 g cm^{-2}, based on run #12 of HP96, implies a diurnal thermal parameter for the N_2 ice slab, Θ_V, of 830. This restricts the temperature range over a day to 0.012 K peak-to-peak (Fig 2E), and the pressure variation to only 1.1%. If subsurface processes were the only processes applicable, then we could constrain the depth to which the solid-gas energy exchange keeps

* I adopt the IAU definition for Pluto's north pole and latitude, which differ from those based on the rotational north pole, used by e.g., Buie et al., (2010a), Grundy and Fink (1996) and L11.

the N_2 slab isothermal by observations of the diurnal variation of pressure. However, as I now show, the atmospheric buffering overwhelms the buffering due to the thermal inertia of the substrate or volatile slab.

For the adopted albedo and emissivity, the temperature is 37.87 K, and the surface pressure is 17.4 μbar, similar to the surface pressure derived by Lellouch et al., (2009). With N_2 ice covering 53% of Pluto's surface, the thermal parameter for the N_2 slab, Θ_V, is 5411. The atmospheric buffering restricts the change in the temperature of the N_2 ice within the volatile slab over a Pluto day to only 0.002 mK (Fig 2F), and the variation in pressure to only 0.25%.

This work implies that if variation is seen in Pluto's atmosphere on short time scales, than the change must be due to something other than changes in surface pressure. One such physical change that can affect a lightcurve is variation in the thermal structure.

4. Comparison with previous work

In analyzing thermal emission from Pluto, Lellouch et al. (2000, 2011b) assume that the N_2 ice temperature is independent of location and time. This work affirms the validity of that assumption.

The formulation of the thermal parameters was constructed in parallel to the work of Spencer et al., (1989), who derived a thermal parameter based on thermal inertia and the equilibrium sub-solar temperature, with a form similar to Θ_S (compare Eq. 12 in this work and Eq. 7 in Spencer et al., 1989). For an equatorial surface element at equinox, $\Theta_S(T_{ss})$, the thermal parameter from Spencer et al. (1989) will be smaller than $\Theta_S(T_0)$, the thermal parameter used here, by $\pi^{3/4} = 2.4$. Fig. 3 shows the surface temperature for an equatorial element at equinox, following Spencer et al., (1989). For all values of $\Theta_S(T_{ss})$, the analytic expressions for a volatile-free area (Eq. 16 and 17) reproduce the phase shift and amplitude of the temperature variation well. However, the analytic expressions only reproduce the mean

temperatures well for $\Theta_S(T_{ss}) > 1.0$ ($\Theta_S(T_0) > 2.4$). This is because the true mean temperature decreases with decreasing Θ_S, a second-order effect not captured in this first-order analysis. While the analytic equations could be extended to include the second-order cross terms (the effect of the temperature variation on the mean temperature), it is complex enough to offer no advantage over numerical integration of the diffusion equation. This is especially true in light of the efficacy of the analytic solution to establish an improved initial condition for numerical integration. Even with $\Theta_S(T_{ss}) = 0.1$, a numeric integration that begins with the analytic solution as the initial condition converges to the exact numeric solution by 1/10 to 1/4 of a period.

INSERT FIG 3 HERE

Trafton and Stern (1983) considered how long it would take half the atmosphere to freeze out if the insolation were instantaneously "turned off," and derive a timescale of $\tau = m_A L / 2\varepsilon\sigma T_V^4$. They present a timescale of 93 Earth days for CH_4 at T_V = 57.8 K, much longer than the 3.2 Earth days of night for Pluto at equinox, and conclude that there is little freezeout overnight. For N_2, with m_A=0.28 g cm^{-2}, this timescale is smaller, 65 Earth days, but still much longer than 3.2 Earth days. The scenario of insolation instantaneously "turning off" is applicable on a seasonal timescale to the case of the disappearance by sublimation of a summer cap, leaving an unilluminated winter cap (HP96).

$$\begin{aligned} \tau_A &= L \frac{m_A}{T_F} \frac{1}{2\varepsilon\sigma T_V^3} && \text{Turning off of insolation, Trafton \& Stern, 1983} \\ \tau_A &= \frac{L}{f} \frac{dm_A}{dT_V} \frac{1}{4\varepsilon\sigma T_V^3} && \text{Relaxation to new equilibrium, this work} \end{aligned} \tag{23}$$

Moore and Spencer (1990) and Spencer and Moore (1992) modeled Triton's seasonal variation including the thermal inertia of the substrate, while Hansen and Paige (1992, 1996) included additionally both the thermal inertia of an isothermal volatile slab and conservation of mass between the volatile slab and the atmosphere. While we can use the above analysis to quantify Pluto's behavior on diurnal timescales, it should be used with caution for seasonal

evolution. One of the simplifying assumptions is that the distribution of volatile ices is static, something that is certainly not the case with Pluto (HP96). However, we can get a rough feel for the relative importance of the various buffering mechanisms by considering an "ice ball," or a world covered entirely with volatiles (Table 3). Here we see the paramount importance of the substrate thermal wave, with the volatile slab and atmospheric buffering playing secondary roles.

INSERT TABLE III HERE

5. Summary and conclusions

I derive an analytic expression for the variation in surface and sub-surface temperature on a world where the pressure is in vapor-pressure equilibrium with surface volatile ices. This is most simply described in terms of three thermal parameters relating to the thermal wave within the substrate, the energy needed to heat an isothermal slab of volatile ice, and the buffering by the latent heat needed to change the atmospheric pressure. One of these thermal parameters is identical in form to that derived by Spencer et al. (1989), and another is closely related to the time constant for thermal collapse derived by Trafton and Stern (1983). Nevertheless, this is the first application of these thermal parameters for calculating an approximate temperature field (temperature as a function of latitude, longitude, depth, and time) for volatile-covered or volatile-free areas on a Pluto-like body.

This approximation can be used as an aid to intuition. If any one of the three thermal parameters is large, or the periodic variation in the solar forcing is small, this approximation can be used for rapid computation of the temperature field. Even for smaller values of the thermal parameters, where the agreement with numerical calculations breaks down, the approximation can be used as an effective initial condition, allowing convergence to the final solution in typically 1/10 to 1/4 of a period.

The analytic model was applied to an example describing Pluto's diurnal variation. For Pluto's current surface pressure (~17 μbar), atmospheric buffering dominates over subsurface effects, and should keep the surface pressure over a Pluto day constant to within 0.2%. Any short-term variation in observations of Pluto's atmosphere are the product of changes in the temperature profile or atmospheric composition, not changes in the surface pressure. Such observations include high-resolution infrared absorption lines or the shape of occultation lightcurves.

Acknowledgement

This work was supported, in part, by funding from NASA Planetary Atmospheres grant NNG06GF32G and the Spitzer project (JPL research support agreement 1368573). This paper was improved by discussions with and critical readings by Marc Buie, Will Grundy, and John Spencer.

References

Assafin, M., J. I. B. Camargo, R. Vieira Martins, A. H. Andrei, B. Sicardy, L. Young, D. N. da Silva Neto, and F. Braga-Ribas 2010. Precise predictions of stellar occultations by Pluto, Charon, Nix, and Hydra for 2008-2015. Astronomy and Astrophysics 515, A32.

Brown, G. N. Jr. and E. T. Ziegler 1980. Vapor pressure and heats of vaporization and sublimation of liquids and solids of interest in cryogenics below 1-atm pressure. Adv, Cryog. Eng. 25, 662-670.

Buie, M. W., and 29 colleagues 2009. Pluto Stellar Occultation on 2008 Aug 25. Bulletin of the American Astronomical Society 41, 562

Buie, M. W., W. M. Grundy, E. F. Young, L. A. Young, and S. A. Stern 2010. Pluto and Charon with the Hubble Space Telescope. I. Monitoring Global Change and Improved Surface Properties from Light Curves. The Astronomical Journal 139, 1117-1127.

Elliot, J. L., and 13 colleagues 1998. Global warming on Triton. Nature 393, 765-767.

Elliot, J. L., and 17 colleagues 2000. The Prediction and Observation of the 1997 July 18 Stellar Occultation by Triton: More Evidence for Distortion and Increasing Pressure in Triton's Atmosphere. Icarus 148, 347-369.

Elliot, J. L., and 28 colleagues 2003. The recent expansion of Pluto's atmosphere. Nature 424, 165-168.

Elliot, J. L., and 19 colleagues 2007. Changes in Pluto's Atmosphere: 1988-2006. The Astronomical Journal 134, 1-13.

Grundy, W. M. 2011. Surface Composition Overview. New Horizons Workshop on Icy Surface Processes, Lowell Observatory, Aug 30-31 2011.

Grundy, W.M. and U. Fink 1996. Synoptic CCD spectrophotometry of Pluto over the past 15 years. Icarus 124, 329–343.

Grundy, W. M. and J. A. Stansberry 2000. Solar Gardening and the Seasonal Evolution of Nitrogen Ice on Triton and Pluto. Icarus 148, 340-346.

Grundy, W. M., L. A. Young, C. B. Olkin, M. W. Buie, and J. A. Stansberry 2009. Observed Spatial Distribution and Secular Evolution of Ices on Pluto and Triton. AAS/Division for Planetary Sciences Meeting Abstracts 41, #06.01

Grundy, W. M. and M. W. Buie 2001. Distribution and Evolution of CH_4, N_2, and CO Ices on Pluto's Surface: 1995 to 1998. Icarus 153, 248-263.

Hansen, C. J. and D. A. Paige 1992. A thermal model for the seasonal nitrogen cycle on Triton. Icarus 99, 273-288.

Hansen, C. J. and D. A. Paige 1996. Seasonal Nitrogen Cycles on Pluto. Icarus 120, 247-265.

Hapke, B. 1993. Theory of reflectance and emittance spectroscopy. Topics in Remote Sensing, Cambridge, UK: Cambridge University Press.

Lellouch, E., B. Sicardy, C. de Bergh, H.-U. Käufl, S. Kassi, and A. Campargue 2009. Pluto's lower atmosphere structure and methane abundance from high-resolution spectroscopy and stellar occultations. Astronomy and Astrophysics 495, L17-L21.

Lellouch, E., C. de Bergh, B. Sicardy, H. U. Käufl, and A. Smette 2011a. High resolution spectroscopy of Pluto's atmosphere: detection of the 2.3 μm CH_4 bands and evidence for carbon monoxide. Astronomy and Astrophysics 530, L4.

Lellouch, E., J. Stansberry, J. Emery, W. Grundy, and D. P. Cruikshank 2011b. Thermal properties of Pluto's and Charon's surfaces from Spitzer observations. Icarus 214, 701-716.

Moore, J. M. and J. R. Spencer 1990. Koyaanismuuyaw - The hypothesis of a perennially dichotomous Triton. Geophysical Research Letters 17, 1757-1760.

Olkin, C. B., L. A. Young, R. G. French, E. F. Young, M. W. Buie, R. R. Howell, J. Regester, C. R. Ruhland, T. Natusch, D. J. Ramm, Pluto's atmospheric structure from the July 2007 stellar occultation. *submitted.*

Owen, T. C., T. L. Roush, D. P. Cruikshank, J. L. Elliot, L. A. Young, C. de Bergh, B. Schmitt, T. R. Geballe, R. H. Brown, and M. J. Bartholomew 1993. Surface ices and the atmospheric composition of Pluto. Science 261, 745-748.

Person, M. J., and 20 colleagues 2010. Pluto's Atmosphere from the July 2010 Stellar Occultation. Bulletin of the American Astronomical Society 42, 983.

Sicardy, B., and 40 colleagues 2003. Large changes in Pluto's atmosphere as revealed by recent stellar occultations. Nature 424, 168-170.

Spencer, J. R. 1990. A rough-surface thermophysical model for airless planets. Icarus 83, 27-38.

Spencer, J. R. and J. M. Moore 1992. The influence of thermal inertia on temperatures and frost stability on Triton. Icarus 99, 261-272.

Spencer, J. R., L. A. Lebofsky, and M. V. Sykes 1989. Systematic biases in radiometric diameter determinations. Icarus 78, 337-354.

Spencer, J. R., J. A. Stansberry, L. M. Trafton, E. F. Young, R. P. Binzel, and S. K. Croft 1997. Volatile Transport, Seasonal Cycles, and Atmospheric Dynamics on Pluto. In Stern, S. A., Tholen, D. J. (Eds.), *Pluto and Charon*, Univ. of Arizona Press, Tucson, pp. 435–473.

Stern, S. A. and L. Trafton 1984. Constraints on bulk composition, seasonal variation, and global dynamics of Pluto's atmosphere. Icarus 57, 231-240.

Trafton, L. 1990. A two-component volatile atmosphere for Pluto. I - The bulk hydrodynamic escape regime. The Astrophysical Journal 359, 512-523.

Trafton, L. and S. A. Stern 1983. On the global distribution of Pluto's atmosphere. The Astrophysical Journal 267, 872-881.

Young, L. A., and 27 colleagues 2008. New Horizons: Anticipated scientific investigations at the Pluto system. Space Science Reviews 140, 93-127.

Young, L., and 14 colleagues 2010. Results from the 2010 Feb 14 and July 4 Pluto Occultations. Bulletin of the American Astronomical Society 42, 982

Young, L., and 10 colleagues 2009. Results from the 2009 April 21 Pluto Occultation. AAS/Division for Planetary Sciences Meeting Abstracts #41 41, #06.05

Young, E. F., and 13 colleagues 2008. Vertical Structure in Pluto's Atmosphere from the 2006 June 12 Stellar Occultation. The Astronomical Journal 136, 1757-1769.

Young, L., and 14 colleagues 2010. Results from the 2010 Feb 14 and July 4 Pluto Occultations. Bulletin of the American Astronomical Society 42, 982.

Tables

Table I. Thermal parameters and their effect on the temperature response

	Thermal parameter	Amplitude factor, a		Phase lag (radian), ψ		Relaxation
	Θ	$\Theta << 4$	$\Theta >> 4$	$\Theta << 4$	$\Theta >> 4$	time scale, τ
Substrate	$\frac{\sqrt{\omega}\langle\Gamma\rangle}{\langle\varepsilon\rangle\sigma T_{V0}^3}$	$1-\frac{\Theta_S}{4\sqrt{2}}$	$\frac{4}{\Theta_S}\left(1-\frac{2\sqrt{2}}{\Theta_S}\right)$	$\frac{\Theta_S}{4\sqrt{2}}$	$\frac{\pi}{4}-\frac{2\sqrt{2}}{\Theta_S}$	$\frac{\langle\Gamma\rangle}{\sqrt{2\omega}}\frac{1}{4\langle\varepsilon\rangle\sigma T_{V0}^3}$
Volatile slab	$\frac{\omega\langle m_{V0}c_V\rangle}{\langle\varepsilon\rangle\sigma T_{V0}^3}$	$1-\frac{\Theta_V}{32}$	$\frac{4}{\Theta_V}\left(1-\frac{8}{\Theta_V^2}\right)$	$\frac{\Theta_V}{4}$	$\frac{\pi}{2}-\frac{4}{\Theta_V}$	$\frac{\langle m_{V0}c_V\rangle}{4\langle\varepsilon\rangle\sigma T_{V0}^3}$
Atmosphere	$\omega\frac{L}{f}\frac{dm_A}{dT_V}\frac{1}{\langle\varepsilon\rangle\sigma T_{V0}^3}$	$1-\frac{\Theta_A}{32}$	$\frac{4}{\Theta_A}\left(1-\frac{8}{\Theta_A^2}\right)$	$\frac{\Theta_A}{4}$	$\frac{\pi}{2}-\frac{4}{\Theta_A}$	$\frac{L}{f}\frac{dm_A}{dT_V}\frac{1}{4\langle\varepsilon\rangle\sigma T_{V0}^3}$

Table II: Example thermal parameters and time constants for Pluto's diurnal cycle

	Assumptions	Thermal parameter	ΔT_V (K)	p_{max}/p_{min}	τ (Earth days)
Unbuffered	Grundy & Fink (1996) map $A_V = 0.8$, $\varepsilon_V = 0.55$, $\Delta = 32.05$ AU, $\phi_0 = -44.25°$ $T_{V0} = 37.89$ K	n/a	4.2	11.7	n/a
Substrate	$\Gamma=1.8\times10^4$ erg cm^{-2} s^{-1} K$^{-1/2}$	$\Theta_S(T_{V0})=36$	0.41	1.27	9.1
Volatile slab	$c_V = 1.3\text{x}10^7$ erg g^{-1} $m_{V0} = 9.5$ g cm^{-2}	$\Theta_V(T_{V0})=830$	0.012	1.011	211
Atmosphere	$L=2.532\text{x}10^9$ erg g^{-1} $f=0.53$ $g=61.9$ cm s^{-2} $dp/dT = 10.36$ μbar/K	$\Theta_A(T_{V0})=5411$	0.0019	1.0015	1375

Table III: Example thermal parameters and time constants for Pluto's seasonal cycle

	Assumptions	Thermal parameter	ΔT_V (K)	p_{max}/p_{min}	τ (Earth years)
Unbuffered	"ice ball" $A_V = 0.8$, $\varepsilon_V = 0.55$, $\Delta = 29.7\text{-}49.1$ AU $T_{V0} = 35.83$ K	n/a	8.9	555	n/a
Substrate	$\Gamma = 2.9\times10^5$ erg cm^{-2} s^{-1} K$^{-1/2}$	$\Theta_S(T_{V0})=5.7$	3.7	11.7	225
Volatile slab	$c_V = 1.3\text{x}10^7$ erg g^{-1} $m_{V0} = 200$ g cm^{-2}	$\Theta_V(T_{V0})=1.5$	3.4	9.3	59
Atmosphere	$L=2.536\text{x}10^9$ erg g^{-1} $f=1$ g=61.9 cm s^{-2} $dp/dT = 3.14$ μbar/K	$\Theta_A(T_{V0})=0.074$	3.4	9.3	2.9

Figures

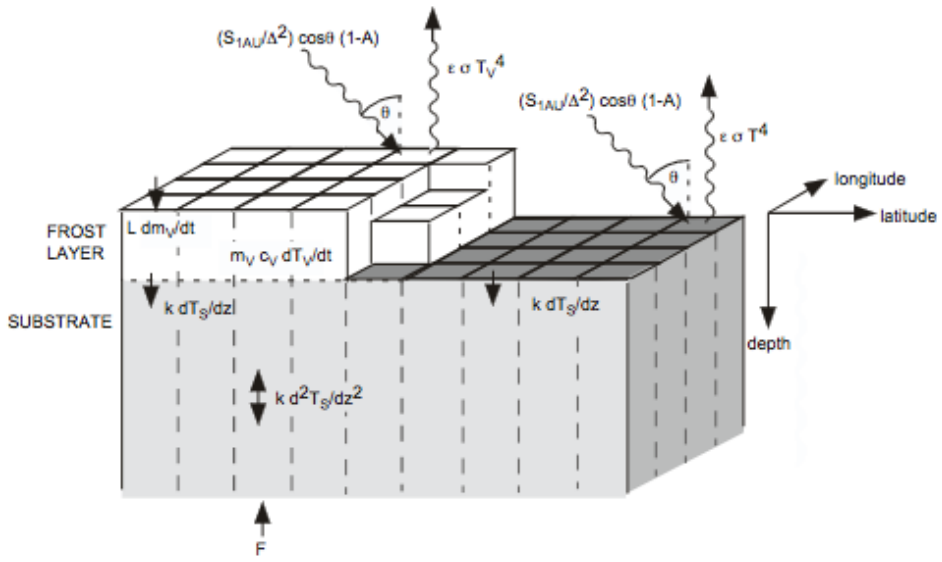

Fig. 1. Schematic of the frost heat balance equation solved by the analytic model (based on Hansen and Paige 1996). Locally, we balance incoming insolation, $S = (S_{1AU}/\Delta^2)\cos\theta(1-A)$, emitted thermal energy $\varepsilon\sigma T^4$, and latent heat of sublimation or condensation, $L\ dm_V/dt$. Additionally we balance heat to and from the substrate, $k\ dT_S/dz$, and the heat capacity of the frost layer, $m_V\ c_V\ dT_V/dt$. All variables except T_V are free to vary with latitude and longitude.

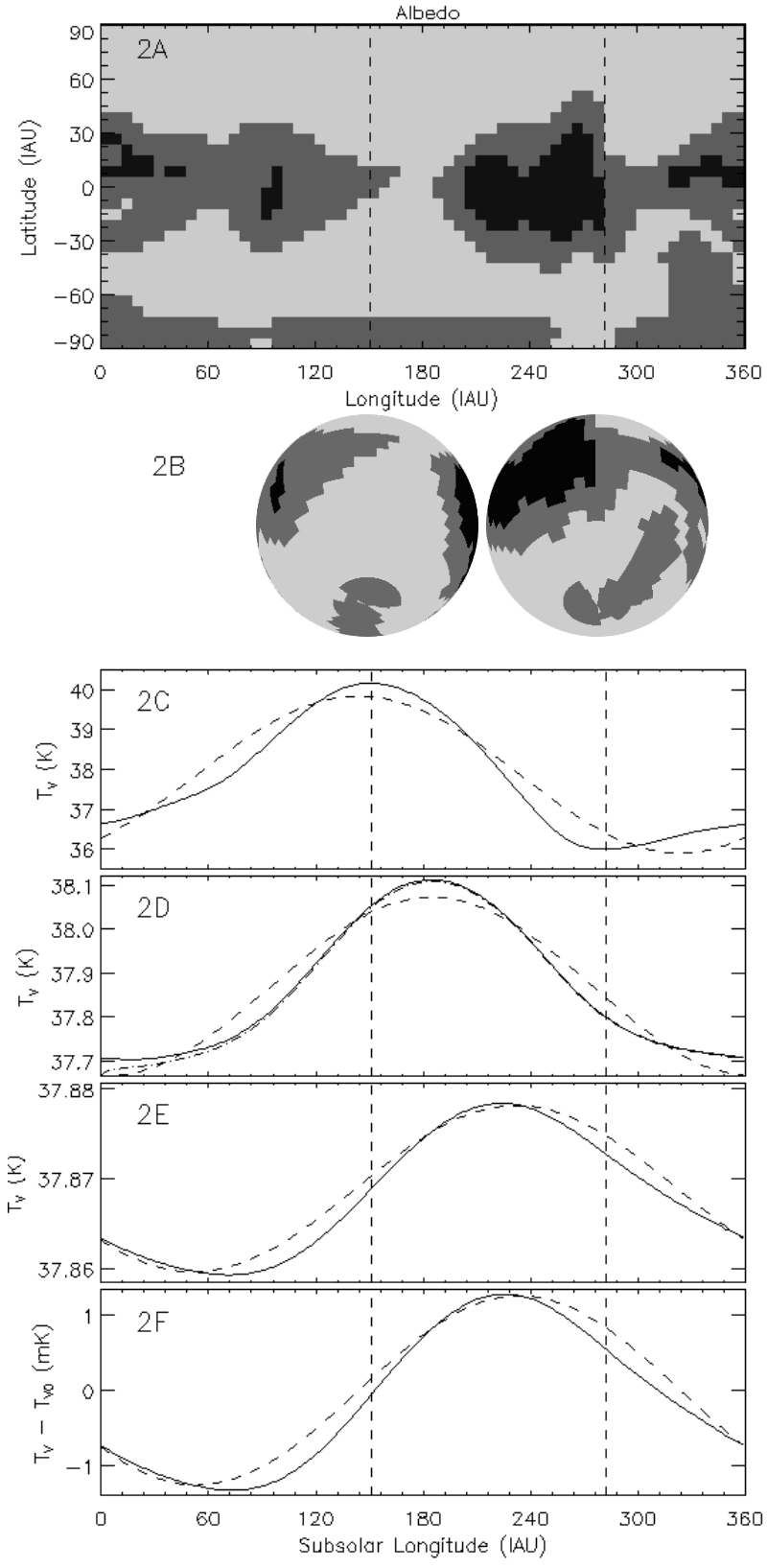
Albedo
2A
Latitude (IAU)
Longitude (IAU)
2B
2C
T_v (K)
2D
T_v (K)
2E
T_v (K)
2F
$T_v - T_{vo}$ (mK)
Subsolar Longitude (IAU)

Fig 2.

Fig. 2. Application to Pluto's diurnal rotation. 2A: Pluto's composition map, based on Grundy and Fink, 1996. The lightest terrains are N_2-rich, and participate in the global exchange of mass and energy. The mid-gray terrains are CH_4-rich, and the darkest terrains are tholins or H_2O. Also marked are the longitudes of minimum and maximum solar insolation (averaged over the frost), 151° and 283°, respectively. (2B) Pluto as seen from the sun in 2011, with a subsolar latitude of -44.25°. The two projections show Pluto when the N_2 ice sees the least insolation (left, 151°), and when it sees the most insolation (right, 283°). (2C) N_2-ice temperature for a surface in instantaneous equilibrium with the insolation. The solid line is the exact solution, and the dashed line is the first-order approximation to a sinusoid. (2D) N_2-icetemperatures, including the effects of a thermal wave within the substrate. The solid line is the numerical integration, and the dashed line is the analytic approximation presented here. The dot-dashed line shows the first period of the numerical solution, using the analytic solution as an initial condition, showing rapid convergence to the final numerical solution. (2E) N_2-icetemperatures, including the buffering needed to heat or cool an isothermal volatile slab. As in 2D, the solid line is the numerical integration, and the dashed line is the analytic approximation. (2F) The difference between the time-varying N_2-ice temperature and its mean, when the atmospheric buffering is also included. As with 2D and 2E, the solid line is the numerical integration, and the dashed line is the analytic approximation.

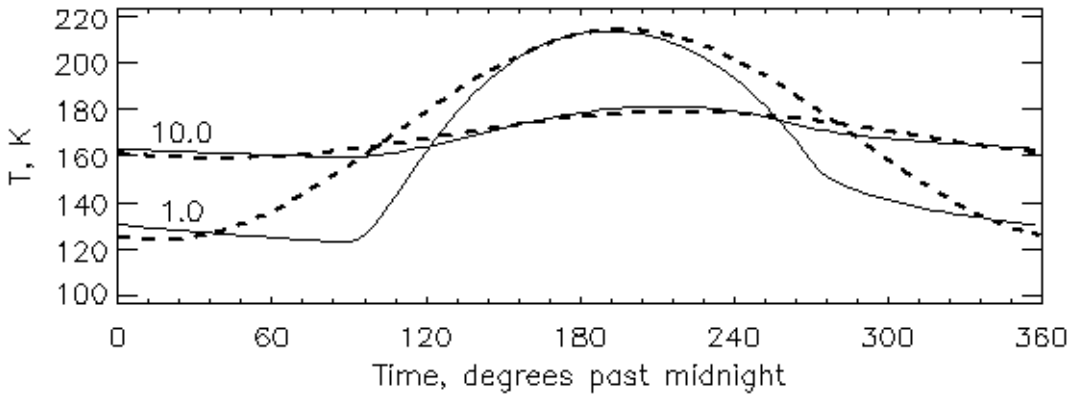

Fig. 3. Comparison of analytic (dashed) vs. numeric (solid) solutions for the surface temperature of frost-free regions, after Spencer et al. (1989). Two cases are plotted, one with $\Theta_S(T_{ss}) = 1$ ($\Theta_S(T_0) = 2.4$) and one with $\Theta_S(T_{ss}) = 10$ ($\Theta_S(T_0) = 24$). Both cases are for an equatorial location for an object at 3 AU, with an albedo of 0.05, an emissivity of 1.0, and a zero sub-solar latitude.

Figure Captions

Fig. 1. Schematic of the frost heat balance equation solved by the analytic model (based on Hansen and Paige 1996). Locally, we balance incoming insolation, $S = (S_{1AU}/\Delta^2)\cos\theta(1-A)$, emitted thermal energy $\varepsilon\sigma T^4$, and latent heat of sublimation or condensation, $L\, dm_V/dt$. Additionally we balance heat to and from the substrate, $k\, dT_S/dz$, and the heat capacity of the frost layer, $m_V\, c_V\, dT_V/dt$. All variables except T_V are free to vary with latitude and longitude.

Fig. 2. Application to Pluto's diurnal rotation. 2A: Pluto's composition map, based on Grundy and Fink, 1996. The lightest terrains are N_2-rich, and participate in the global exchange of mass and energy. The mid-gray terrains are CH_4-rich, and the darkest terrains are tholins or H_2O. Also marked are the longitudes of minimum and maximum solar insolation (averaged over the frost), 151° and 283°, respectively. (2B) Pluto as seen from the sun in 2011, with a subsolar latitude of -44.25°. The two projections show Pluto when the N_2 ice sees the least insolation (left, 151°), and when it sees the most insolation (right, 283°). (2C) N_2-ice temperature for a surface in instantaneous equilibrium with the insolation. The solid line is the exact solution, and the dashed line is the first-order approximation to a sinusoid. (2D) N_2-icetemperatures, including the effects of a thermal wave within the substrate. The solid line is the numerical integration, and the dashed line is the analytic approximation presented here. The dot-dashed line shows the first period of the numerical solution, using the analytic solution as an initial condition, showing rapid convergence to the final numerical solution. (2E) N_2-icetemperatures, including the buffering needed to heat or cool an isothermal volatile slab. As in 2D, the solid line is the numerical integration, and the dashed line is the analytic approximation. (2F) The difference between the time-varying N_2-ice temperature and its mean, when the atmospheric buffering is also included. As with 2D and

2E, the solid line is the numerical integration, and the dashed line is the analytic approximation.

Fig. 3. Comparison of analytic (dashed) vs. numeric (solid) solutions for the surface temperature of frost-free regions, after Spencer et al. (1989). Two cases are plotted, one with $\Theta_S(T_{ss}) = 1$ ($\Theta_S(T_0) = 2.4$) and one with $\Theta_S(T_{ss}) = 10$ ($\Theta_S(T_0) = 24$). Both cases are for an equatorial location for an object at 3 AU, with an albedo of 0.05, an emissivity of 1.0, and a zero sub-solar latitude.